Regulatory coiled-coil domains promote head-to-head assemblies of AAA+ chaperones essential for tunable activity control

Marta Carroni[1,5,*], Kamila B. Franke[2,5], Michael Maurer[2], Jasmin Jäger[2], Ingo Hantke[3], Felix Gloge[4], Daniela Linder[2], Sebastian Gremer[2], Kürşad Turgay[3], Bernd Bukau[2,*] and Axel Mogk[2,*]

[1] Swedish Cryo-EM Facility, Science for Life Laboratory Stockholm University, Box 1031, SE-171 21 Solna, Sweden

[2] Center for Molecular Biology of the University of Heidelberg (ZMBH) and German Cancer Research Center (DKFZ), DKFZ-ZMBH Alliance, Im Neuenheimer Feld 282, D-69120 Heidelberg, Germany

[3] Institute for Microbiology, Leibniz Universität Hannover, D-30167 Hannover, Germany

[4] Wyatt Technology Europe, Hochstrasse 12a, 56307 Dernbach, Germany

[5] these authors contributed equally to this work

[*] corresponding authors

Correspondence:

marta.carroni@scilifelab.se

a.mogk@zmbh.uni-heidelberg.de

bukau@zmbh.uni-heidelberg.de

Abstract

Ring-forming AAA+ chaperones exert ATP-fueled substrate unfolding by threading through a central pore. This activity is potentially harmful requiring mechanisms for tight repression and substrate-specific activation. The AAA+ chaperone ClpC with the peptidase ClpP forms a bacterial protease essential to virulence and stress resistance. The adaptor MecA activates ClpC by targeting substrates and stimulating ClpC ATPase activity. We show how ClpC is repressed in its ground state by determining ClpC cryo-EM structures with and without MecA. ClpC forms large two-helical assemblies that associate via head-to-head contacts between coiled-coil middle domains (MDs). MecA converts this resting state to an active planar ring structure by binding to MD interaction sites. Loss of ClpC repression in MD mutants causes constitutive activation and severe cellular toxicity. These findings unravel an unexpected regulatory concept executed by coiled-coil MDs to tightly control AAA+ chaperone activity.

Introduction

AAA+ (ATPase associated with a variety of cellular activities) proteins control a multitude of essential cellular activities including DNA replication and recombination, protein transport and quality control, among many others [1]. AAA+ proteins convert the energy derived from ATP hydrolysis into a mechanical force to remodel bound substrates. ATP binding and hydrolysis is mediated by the conserved AAA domain, which also mediates AAA+ protein oligomerization typically into hexameric assemblies harboring a central channel. Substrate remodeling involves a threading activity into the central channel mediated by mobile loops that bind substrates and pull them upon nucleotide-induced motions [2,3]. AAA+ proteins gain functional diversity by extra domains that are either fused to or inserted into AAA domains. Extra domains enable targeting of specific substrates but they can also globally control AAA+ protein activity [4].

AAA+ proteins are key players in protein quality control by targeting misfolded and aggregated proteins to degrading and refolding pathways. ClpB/Hsp104 reactivates aggregated proteins in concert with a cognate Hsp70 system [5,6]. Other AAA+ proteins (e.g. ClpX, Rpt1-6) associate with peptidases (e.g. ClpP, 20S proteasome) to form AAA+ proteases, feeding protein substrates into associated proteolytic chambers for degradation [7,8]. The unfolding activity of AAA+ proteins can, however, also be deleterious to cells, in particular if linked to protein degradation, and therefore needs to be tightly controlled. Accordingly, loss of the control mechanisms of AAA+ protein activity in mutant proteins can lead to cell death [9-11].

A high degree of substrate selectivity is equally important to ensure proper functioning of AAA+ proteins and to prevent deleterious activities. Substrate specificity is achieved by adaptor proteins, which bind selective substrates and target them to the AAA+ partner chaperone. Their functions can be additionally controlled by post-translational modifications [12], counteracting anti-adaptors [13,14] or degradation [15]. Adaptor proteins can furthermore regulate the ATPase activity of AAA+ proteins and couple substrate delivery to ATPase activation [9,16].

Activity control and adaptor action requires the ATPase activity to be repressed in the ground state, which is key to AAA+ chaperone mode of action. Repression can be achieved by regulatory coiled-coil domains inserted into an AAA module. In the ClpB/Hsp104 disaggregase a long coiled-coil middle domain (MD), consisting of two wings, is forming a repressing belt around the AAA ring to reduce ATPase activity [17,18]. Adjacent MDs bind to each other by head-to-tail interactions keeping the regulatory domains in place. ATPase repression is relieved by MD dissociation and binding to Hsp70 adaptors that prevent reassociation of MDs with the ClpB/Hsp104 ring [9,19,20].

The bacterial AAA+ chaperone ClpC associates with the peptidase ClpP to form a central proteolytic machinery of Gram-positive bacteria. The ClpC-ClpP machinery acts in regulatory and general proteolysis, controlling multiple cellular pathways and differentiation processes and is crucial for bacterial stress resistance and virulence [21-28]. ClpC activity crucially relies on cooperation with adaptor proteins including MecA, that target specific substrates while concurrently stimulating ClpC ATPase activity [15,16,21,29]. MecA binds to N-terminal and middle domains of each ClpC subunit forming a separate layer on top of the

ClpC AAA ring [30]. How ClpC is kept inactive in adaptor absence, and how the adaptor activates the ATPase is largely unknown. Furthermore, ClpC harbors a coiled-coil MD consisting only of a single wing, as opposed to the two-wing MD of ClpB/Hsp104. A potential regulatory function of the ClpC MD has not been investigated, but its smaller size as compared to the ClpB/Hsp104 MD implies it must act differently if involved in ClpC activity control. Understanding ClpC regulation is particularly relevant as AAA+ protease machines including ClpC have attracted considerable attention as targets for antibacterial action in recent years [31]. Overruling AAA+ protease control by small molecules can lead to constitutive uncontrolled and toxic activation as best exemplified by acyldepsipeptide antibiotics of the ADEP class targeting the ClpP peptidase. ADEP-activated ClpP causes aberrant protein degradation and even allows for eradication of *Staphylococcus aureus* persister cells [32-34]. Understanding ClpC activity control therefore might open new avenues for antibiotics development.

Here, we report on an unexpected mode of AAA+ chaperone control involving transition between an inactive resting state and a functional hexamer as revealed by determining the cryoEM-structures of *S. aureus* ClpC in absence and presence of MecA. The ClpC resting state is composed of two helical ClpC assemblies stabilized by head-to-head MD interactions. MecA prevents MD interactions and thereby converts ClpC into a canonical and active hexamer.

Results

The ClpC M-domain represses ClpC activity

To study the function of the M-domain (MD) in ClpC activity control we first purified *S. aureus* ClpC/ClpP and demonstrated functionality by determining high-proteolytic activity in presence of the adaptor MecA (**Fig. 1**). Next, we created a series of ClpC MD variants by mutating conserved residues not involved in coiled-coil structure formation (**Supplementary Fig. 1A**). Additionally, we replaced the entire MD (N411-K457) by a di-glycine linker, allowing MD deletion without interfering with folding of the AAA-1 domain. Proteolytic activities of MD mutants were determined using Fluorescein-labeled casein (FITC-casein) as constitutively misfolded model substrate in absence and presence of MecA (**Fig. 1A/B, Supplementary Fig. 1B**). ClpC wild type (WT) together with ClpP exhibited only a low proteolytic activity in absence of MecA and FITC-casein degradation rates were 20-fold increased upon adaptor addition. In contrast, most MD mutants enabled for adaptor-independent FITC-casein proteolysis to varying degrees. ClpC-F436A, ClpC-R443A and ClpC-D444A showed highest activities with degradation rates close to those determined for ClpC WT plus MecA (**Fig. 1A/B**). Similarly, MD deletion strongly increased ClpC activity, indicating that the single point mutants reflect a loss of M-domain function. MecA presence still stimulated FITC-casein degradation by ClpC MD mutants except F436A and ΔM, consistent with the crucial function of F436 in MecA binding (**Supplementary Fig. 1B**) [30].

FITC-casein degradation by activated ClpC M-domain mutants (F436A, ΔM) required ATP hydrolysis and was not observed in presence of ATPγS

(**Supplementary Fig. 1C**). Complete degradation of FITC-casein by ClpC-F436A was confirmed by SDS-PAGE (**Supplementary Fig. 2**), while ClpC WT required MecA to exhibit proteolytic activity. Here, we also noticed MecA autodegradation once FITC-casein was digested, in agreement with former findings for the *B. subtilis* ClpC/MecA system [15,16,29]. We infer that ClpC MD mutants exhibit high, adaptor-independent proteolytic activities, qualifying the M-domain as a negative regulatory element.

To further investigate a repressing function of the ClpC MD we determined GFP-SsrA degradation activities of selected ClpC MD mutants exhibiting highest FITC-casein degradation activities (F436A, R443A, ΔM). GFP-SsrA harbors the 11-meric SsrA tag, which is recognized by AAA+ chaperones pore sites [35-37]. GFP-SsrA degradation requires application of high unfolding force in contrast to FITC-casein, which is constitutively unfolded. ClpC WT/ClpP efficiently degraded GFP-SsrA in a MecA-dependent manner (**Fig. 1C**). Surprisingly, ClpC MD mutants did hardly exhibit autonomous degradation of GFP-SsrA in contrast to FITC-casein. ClpC-R443A was partially stimulated upon MecA addition demonstrating that the M-domain mutant can process GFP-SsrA in principle (**Supplementary Fig. 3A**). We speculated that differences in GFP-SsrA and FITC-casein binding modes might be the cause of the different degradation activities of ClpC MD mutants. Hsp100 N-domains contribute to casein binding [38,39] while their position on top of the AAA-1 ring and central pore site could impede GFP-SsrA binding. We therefore determined GFP-SsrA degradation activities of N-domain deleted ΔN-ClpC and respective MD mutants (**Fig. 1D**). GFP-SsrA remained stable in presence of ΔN-ClpC/ClpP, however, the substrate was rapidly degraded by ΔN-

ClpC-F436A, ΔN-ClpC-R443A and ΔN-ClpC-ΔM (+ ClpP) and degradation rates were identical to those determined for ClpC WT/ClpP with MecA (**Fig. 1E**). We did not test for GFP-SsrA degradation by ΔN-ClpC/ClpP in presence of MecA, as the N-domain is essential for MecA binding [30,40,41]. GFP-SsrA degradation by activated ΔN-ClpC M-domain mutants relied on ATP hydrolysis and remained specific as the substrate variant GFP-SsrA-DD was not degraded (**Supplementary Fig. 3B**). Here, the two C-terminal alanine residues of the SsrA tag are replaced by aspartate residues, obstructing binding to the AAA+ chaperone pore site [42]. This documents that MD mutations boost ClpC unfolding activity in absence of adaptor without altering general substrate specificity.

ClpC M-domain mutants exhibit increased basal ATPase activities

B. subtilis ClpC activation by adaptors involves strong stimulation of ClpC ATPase activity [21,29,41], which we confirm here for *S. aureus* ClpC and MecA (**Fig. 2A**). ClpC WT exhibits a very low basal ATPase activity (0.4 ATP/min/monomer), rationalizing its poor standalone degradation activity. Notably, all activated MD mutants (F436A, R443A, ΔM) exhibited strongly increased basal ATPase activities (3.3 – 5.4 ATP/min/monomer) that were further increased by substrate casein (1.64 – 2.47-fold stimulation) in contrast to ClpC WT (**Fig. 2A/B**). Casein-stimulated ClpC MD mutants reached 33% of total ATPase activity determined for MecA-activated ClpC WT. N-domain deletion also increased basal ATPase activity of ΔN-ClpC. Combining ΔN-ClpC with M-domain mutants had an additive stimulatory effect on ATPase activities, suggesting that the underlying mechanisms are distinct from one another (**Fig. 2A**). We infer increased basal

187 ATPase activities of ClpC MD mutants can explain adaptor-independent
188 substrate degradation. However, ATPase activation alone is not sufficient to
189 explain ClpC activation as ΔN-ClpC did not allow degradation of GFP-SsrA despite
190 having increased basal ATPase activity. This indicates specific consequences of
191 MD mutations on ClpC conformation and activity.

192

193 **Head-to-head interactions of M-domains mediate formation of an inactive**
194 **ClpC resting state**

195 To understand the structural basis underlying the control of ClpC activity by the
196 MD, we determined the cryo-EM structures of *S. aureus* ClpC with and without its
197 activator MecA in the presence of ATPγS. The structure of ClpC on its own was
198 solved at 8.4 Å resolution using ~ 90.000 collected particles (**Supplementary**
199 **Fig. 4A**). Surprisingly, raw images and subsequent 2D classification revealed
200 immediately that ClpC assumes a conformation different from the canonical
201 hexameric arrangement of AAA+ proteins (**Supplementary Fig. 4B/C**). Attempts
202 of 3D classification and refinement using the existing ClpC-MecA structures [30,43]
203 failed to give a refined map, indicating that on its own, ClpC assumes a
204 substantially different conformation. Indeed, reconstructions revealed that ClpC
205 without MecA assembles into an almost decameric assembly made of two open
206 spirals that interact via head-to-head contacts mainly mediated by the MDs (**Fig.**
207 **3A/B, Supplementary Fig. 4D**). Continuous spiraling of AAA+ proteins is often
208 observed in X-ray structures [17,18,44,45] and ClpC half spirals are similar to these
209 crystal packings. However, the ClpC double spiral is completely open on one side
210 (**Fig. 3A/B, Supplementary Movie1**) giving a cradle-like molecule with the

211 peripheral subunits more mobile than the core ones, as shown by lower local
212 resolution (**Supplementary Fig 4E**). Additionally, high-threshold noise on the
213 open part of the spiral indicates higher dynamics of this region, suggesting
214 exchange of subunits. Accordingly, for peripheral ClpC subunits there is not
215 sufficient density to account for all ClpC domains. The overall subdomain
216 organization within the ClpC protomer is similar to that of the ClpC-MecA crystal
217 structures, however domain positions and interactions are different. The AAA+
218 domains are staggered with a rise of ~ 20 Å per subunit (**Fig. 3B**). N-domains
219 domains are packed between MDs and are displaced so that they lie on top of the
220 adjacent small AAA1 subdomain (**Fig. 3B/C**). The MDs coiled-coils constitute the
221 backbone of the spiral and mediate the spiral head-to-head contacts, which
222 involve residues F436, R443 and D444 providing a structural rationale for the
223 activated states of respective MD mutants (**Fig. 3D**).

224 We envision the helical ClpC assembly as a dynamic inactive resting state, which
225 will interfere with substrate binding, association of the ClpP peptidase and
226 interaction with adaptor proteins. Furthermore, the spiral arrangement of the
227 AAA+ domains results in a displacement of most trans-acting arginine-fingers
228 away from the adjacent nucleotide pocket (**Supplementary Fig. 4F**), thereby
229 affecting ATP hydrolysis and explaining the low ATPase activity of ClpC WT.

230 The *S. aureus* ClpC-MecA cryo-EM map was reconstructed at 10 Å resolution with
231 ~26,000 particles, (**Supplementary Fig. 5A-D**) and shows the classical hexameric
232 assembly previously described [30,43], with MecA interacting with both the MD and
233 the N-domain of ClpC. Additional extra density caps the hexamer and accounts
234 for the N-terminal domain of MecA, whose structure is unknown. Automatic

235 flexible fitting revealed that the hexamer is slightly asymmetric with 5 out of 6
236 subunits more defined (**Fig. 3E**), similar to the AAA+ protein Vps4 [46]. From the
237 resting to the MecA-bound state the N-domains undergo a 45° rotation that
238 repositions the MecA-binding loop region from being blocked by the MD of the
239 neighbouring subunit to be available and engaged in MecA binding
240 (**Supplementary Fig. 5 E/F**). Additionally, binding of MecA to MDs breaks head-
241 to-head MD contacts and is therefore expected to prevent formation of the ClpC
242 resting state.

243 Taken together, our structures of ClpC alone or in complex with MecA show a
244 dramatic reorganization from a helical resting state to a planar canonical AAA+
245 hexamer, explaining ClpC activation by the adaptor MecA. Intermolecular head-
246 to-head contacts of MDs form the backbone of the ClpC resting state, qualifying
247 the MD as crucial negative regulatory element consistent with MD mutant
248 characterization.
249

250 **MecA abrogates head-to-head M-domain interactions**

251 To demonstrate direct head-to-head contacts of ClpC MDs we introduced
252 cysteine residues at the tip of the MD (E435C, E437C) to probe for site-specific
253 disulfide crosslinking. These mutations were introduced into ClpC-C311T to
254 avoid interference of the endogenous Cys311 residue. ClpC-C311T/E435C and
255 ClpC-C311T/E437C were active in MecA-dependent protein degradation under
256 reducing conditions (**Supplementary Fig. 6A**). Formation of crosslink products
257 under oxidizing conditions that were fully reverted by addition of reducing agent
258 was observed for ClpC-C311T/E437C but not for ClpC-C311T/E435C and the

ClpC-C311T control (**Supplementary Fig. 6B**). This documents specificity of disulfide crosslinking and agrees well with the ClpC resting state model, showing E437 residues of two interacting M-domains are facing one another while E435 residues are oriented in opposite directions (**Supplementary Fig. 6B**). E437C disulfide crosslinking was most efficient in absence of nucleotide or presence of ADP and ATP, and less efficient in presence of ATPγS (**Supplementary Fig. 6C**). Importantly, ClpC-E437C crosslinking in presence of MecA was strongly reduced (**Fig. 4A**), consistent with MecA binding to MDs preventing head-to-head MD interactions. Similarly, crosslinking efficiency was reduced for ClpC-F436A/E437C, indicating a crucial contribution of F436 to intermolecular MD contacts (**Fig. 4B**), consistent with the ClpC WT cryo-EM structure.

Obstructing head-to-head M-domain contacts allows for ClpC hexamer formation

To provide biochemical support for the formation of a large, inactive ClpC resting state we employed chemical crosslinking and size exclusion chromatography. We used the ATPase-deficient ClpC-E280A/E618A variant (referred to as ClpC-DWB), harboring mutated Walker B motifs in both AAA+ domains allowing for ATP binding but not hydrolysis, facilitating analysis of adaptor or substrate impact on ClpC assembly. We first determined sizes of ClpC assemblies by glutaraldehyde crosslinking (**Fig. 5A**). ClpC-DWB was crosslinked to very large assemblies that were just entering the separating gel in SDS-PAGE in absence and presence of ATP (**Fig. 5A**). Addition of MecA allowed for formation of a smaller high molecular weight complex similar in size to crosslinked ClpB hexamers that were

283 used as reference (**Fig. 5A**). Presence of MecA in the crosslinked ClpC-DWB
284 complexes was confirmed by western-blot analysis (**Supplementary Fig. 7**).
285 ClpC-F436A-DWB stayed monomeric in absence of nucleotide, indicating that
286 large assemblies observed for ClpC-DWB rely entirely on MD contacts (**Fig. 5A**).
287 ClpC-F436A-DWB crosslinking in presence of ATP caused formation of defined
288 ClpC-F436A-DWB complexes that were similar in size to crosslinked ClpB
289 hexamers. These findings confirm the predicted critical contribution of the MD to
290 formation of a large resting state and the role of MecA in converting this
291 assembly into a functional hexamer.

292 We next analyzed sizes of ClpC complexes by size exclusion chromatography (**Fig.**
293 **5B, Supplementary Fig. 8A**). In absence of ATP ClpC-DWB showed a broad
294 elution profile, suggesting formation of variable assemblies ranging from
295 monomers to hexamers. ATP addition caused formation of larger ClpC
296 assemblies that eluted prior to ClpB hexamers and a 670 kDa standard protein,
297 suggesting formation of ClpC complexes larger than hexamers (**Fig. 5B,**
298 **Supplementary Fig. 8A**). This was confirmed by static light scattering (SLS)
299 measurements, revealing a molecular mass of ≈ 956 kDa corresponding to a
300 decameric complex, consistent with cryoEM analysis (**Supplementary Fig. 8B**).
301 Presence of MecA sharpened the ClpC elution profile and shifted ClpC-DWB
302 fractions to later elution volumes right after the 670 kDa standard protein and
303 now overlapping with ClpB hexamers (**Fig. 5B, Supplementary Fig. 8A**).
304 Quantification of co-eluting MecA suggests the formation of a 1:1 ClpC:MecA
305 complex, consistent with the binding stoichiometry determined for *B. subtilis*
306 ClpC/MecA complexes and mass determination by SLS (767 kDa)

(**Supplementary Fig. 8B**)[30,40]. This indicates that MecA binding shifts ClpC from a large, non-hexameric assembly to a $ClpC_6/MecA_6$ complex. We next analyzed the elution profile of ClpC-DWB-F436A. In absence of ATP the MD mutant eluted as defined species right at the elution volume of a 158 kDa standard protein suggesting formation of monomers/dimers (**Fig. 5B**). This indicates that the formation of larger assemblies noticed for ClpC WT (- ATP) depends on the M-domain, consistent with results from glutaraldehyde crosslinking (**Fig. 5A**) Unexpectedly, ClpC-DWB-F436A showed a broad elution profile upon ATP addition. While the ClpC-DWB-F436A peak fraction eluted right after the 670 kDa standard, larger assemblies at earlier elution volumes were also present. We speculated that activated ClpC MD mutants might be capable of recognizing themselves as substrate resulting in formation of larger complexes and explaining the elution profile. Indeed, we observed autodegradation of ClpC-F436A, ClpC-R443A and ClpC-ΔM but not ClpC WT in presence of ClpP (**Supplementary Fig. 9**). To prevent self-recognition of ClpC-DWB-F436A we repeated the size exclusion analysis in presence of substrate casein excess (**Fig. 5B**). Presence of casein sharpened the ClpC-DWB-F436A elution profile that was comparable to ClpC-DWB/MecA complexes and distinct from ClpC-DWB, suggesting hexamer formation, which was confirmed by mass determination by SLS (587 kDa). In contrast, casein addition did not cause formation of smaller ClpC-DWB complexes (**Supplementary Fig. 8B**). To further prove ClpC-F436A hexamer formation, a small cryo-EM dataset of ClpC-F436A with casein and ATPγS was collected and analyzed via 2D classification. Classes indicate that the ClpC-F436A assembles in an hexamer similar to ClpC WT with MecA (**Fig. 5C**).

Together our findings demonstrate that ClpC-DWB forms large, non-hexameric assemblies in a MD dependent manner, supporting the derived ClpC WT cryo-EM structure. This large ClpC-DWB assembly should neither allow for efficient substrate binding nor association with the ClpP peptidase. This prediction was confirmed by size exclusion chromatography showing poor interaction with ClpP and negligible binding to substrate FITC-casein (**Fig. 5D, Supplementary Fig. 8C**). In contrast, efficient binding to FITC-casein and ClpP was observed upon addition of MecA and for ClpC-DWB-F436A (- MecA) (**Fig. 5d, Supplementary Fig. 8C**). These findings were further confirmed by monitoring FITC-casein binding by anisotropy measurements (**Supplementary Fig. 8D/E**).

M-domain activity control of ClpC is crucial for cellular viability

ClpC MD mutants allow for adaptor-independent and thus constitutive and uncontrolled ClpC activity. We wondered whether this loss of ClpC activity control has physiological consequences and co-expressed *S. aureus* ClpC WT, ΔN-ClpC and respective F436A mutants from an IPTG-regulated promoter together with *S. aureus* ClpP in *E. coli* cells. This strategy allowed us to only monitor potential toxic effects of ClpC M-domain mutants without interference by loss of endogenous functions of ClpC/MecA in *S. aureus* cells. Levels of ClpC variants were similar after 1 h of IPTG-induced protein production (**Supplementary Fig. 10A**). In case of ClpC-F436A we noticed accumulation of a degradation product upon ClpP coexpression, as also observed *in vitro* (**Supplementary Fig. 9**), suggesting autoprocessing. We observed strong toxicity upon expression of ΔN-ClpC-F436A at all temperatures tested while ClpC-F436A expression became

lethal at 37°C and 40°C (**Fig. 6A**). Toxicity of ClpC MD mutants was much higher as compared to ClpC-WT and ΔN-ClpC, indicating an essential cellular need for ClpC repression by MDs. Furthermore, toxicity of ClpC MD mutants was dependent on coexpression of *S. aureus* ClpP, suggesting that uncontrolled protein degradation caused by constitutively activation results in cell death (**Supplementary Fig. 10B**).

To further corroborate our findings we explored the physiological consequences of the same ClpC MD mutation in *B. subtilis*. Here, we deleted the chromosomal copy of the *clpC* gene (*clpC::tet*) and re-integrated either *clpC wt* or *clpC-F436A* at the *amyE*-locus under IPTG control. Expression of *clpC-F436A* but not *clpC wt* in presence of 100 μM IPTG was highly toxic at all temperatures (30°C – 50°C) (**Fig. 6B**). Levels of ClpC-wt and ClpC-F436A produced after IPTG addition in cells cultured in liquid medium were comparable, excluding differences in protein levels as reason for toxicity (**Supplementary Fig. 10C**). Importantly, growth of *clpC::tet* cells was not impaired, demonstrating that toxicity of ClpC-F436A reflects a gain-of-function phenotype and is not caused by loss of adaptor interaction (**Fig. 6B**). Together these findings demonstrate an essential role of MD mediated activity control for cellular viability.

The Hsp100 family members ClpE and ClpL harbor a coiled-coil MD that is similar in size to the ClpC MD and also displays some sequence homology. Notably, F436 and R443, identified here as key MD residues in ClpC activity control, are largely conserved in ClpE and ClpL M-domains (**Fig. 6C**). This suggests that the role of M-domains as crucial negative regulators of Hsp100 activity is conserved in other family members. To test for a conserved regulatory

function we generated the *B. subtilis* ClpE-Y344A MD mutant corresponding to ClpC-F436A. *clpE wt* and *clpE-Y344A* copies were integrated at the *amyE*-locus in *B. subtilis* wild type cells under control of an IPTG-regulatable promoter. *B. subtilis* cells do hardly express endogenous *clpE* at non-stress conditions [47,48] thereby allowing mutant analysis without interference of ClpE WT copies. Expression of *clpE-Y344A* but not *clpE wt* in presence of 100 μM IPTG was highly toxic to *B. subtilis* cells at all temperatures tested (30°C – 50°C) (**Fig. 6D**). ClpE WT and ClpE-Y344A were produced to similar levels underscoring that toxicity is caused by deregulation of the ClpE MD mutant (**Supplementary Fig. 10D**). This suggests that ClpE MDs are also essential to downregulate ClpE activity preventing cellular toxicity.

Discussion

In the presented work we established a new mechanism of activity control of ClpC, a central AAA+ chaperone widely distributed among Gram-positive bacteria. We show that coiled-coil MDs control ClpC activity in a unique manner by sequestering ClpC molecules in an inactive resting state.

Our findings extend the role of coiled-coil MDs as regulatory devices controlling AAA+ protein activity. MDs of the ClpB/Hsp104 disaggregases function as molecular toggles, which are crucial for AAA+ protein repression in the ground state and activation by an Hsp70 partner chaperone [9,18-20,49] (**Fig. 7**). Repression by ClpB/Hsp104 MDs relies on formation of a repressing belt around a canonical AAA+ ring by interacting with AAA-1 domains and neighboring MDs.

Intermolecular head-to-tail contacts between long MDs (~ 120 residues forming two wings) are crucial to keep MDs in a horizontal, repressing conformation [17] (**Fig. 7**). Hsp70 binding to the tip of one wing breaks MD interactions and leads to ClpB activation.

ClpC MDs cannot function in the same manner due to their reduced size (~ 50 residues forming a single wing), which is too short to span the distance between neighboring subunits in a hexameric assembly. Instead, ClpC MDs form intermolecular head-to-head contacts allowing docking of two layers of ClpC molecules arranged in a helical conformation (**Fig. 7**). We define this large ClpC assembly as inactive resting state, as it strongly restricts binding of substrates, ClpP and adaptor proteins and does not allow for efficient ATP hydrolysis. The interaction surface of MDs is limited (50 $Å^2$) suggesting that the ClpC storage state is not stable but dynamic, in agreement with our structural and biochemical analysis. This will open the route for ClpC activation upon dissociation of ClpC molecules from the resting structure, liberating MDs and N-domains for binding to activating MecA or other adaptors. Additionally, MecA might bind to peripheral subunits of the ClpC storage state causing their displacement. ClpC MDs thereby function as molecular switches, similar to ClpB/Hsp104 MDs, ensuring repression in the ground state and allowing for activation in presence of substrate recruiting adaptors (**Fig. 7**). This dual activity is best illustrated for MD residue F436 located at the tip of the coiled-coil structure. F436 is essential for both, intermolecular MD interaction and MecA binding (**Fig. 7**). The N-terminal domain appears to play an additional role in this switch of

conformations, by going from a more hidden position in between MDs in the resting state to a more exposed one, available to MecA or other adaptors.

Our newly derived model of *S. aureus* ClpC activity control differs from a former one, showing that *B. subtilis* ClpC is monomeric and requires MecA for hexamer formation [40]. We realize that former ClpC analysis was performed in presence of high salt concentrations (300 mM NaCl), which likely interfere with MD head-to-head contacts involving charged residues (R443, D444). A regulatory model involving only monomer-hexamer transitions cannot explain activation and severe cellular toxicity of ClpC MD mutants shown here in *E. coli* and *B. subtilis* cells. However, we suggest that the oligomerization dependence of ClpC on MecA at high salt concentrations might represent a fail-safe system ensuring adaptor-dependent ClpC activation under conditions that do not allow for resting state formation (e.g. salt stress).

Once formed the hexameric $ClpC_6/MecA_6$ complex is stable and does not dissociate spontaneously, raising the question how ClpC activation is turned off. Adaptor proteins are targeting themselves for autodegradation by ClpC/ClpP if substrates are no longer available [15,29,50]. This mechanism couples substrate availability with ClpC activation and ensures fast ClpC inactivation in absence of substrate by causing dissociation of ClpC hexamers into monomers that are subsequently sequestered in the resting state. Notably, other chaperone machineries including the Hsp70 member BIP [51] and the AAA+ protein Rca [52] also form large, inactive resting states that are converted into active species depending on substrate availability. Sequestration of chaperones therefore

448 seems a more widespread activity to tune their activities according to the
449 physiological need.

450 Constitutively activated ClpC MD mutants exert strong toxicity in *E. coli* and *B.*
451 *subtilis* cells, demonstrating an essential physiological need to tightly control
452 ClpC function. We assume that overhasty protein degradation by deregulated
453 ClpC/ClpP complexes of e.g. newly synthesized proteins or secretory proteins,
454 which did not yet reach their native structures or cellular compartment, leads to
455 cell death.

456 Homologous MDs are present in the AAA+ protein family members ClpE and
457 ClpL and key residues driving formation of the ClpC resting state are
458 evolutionary conserved. We show that mutating a key regulatory MD residue of
459 ClpE also causes cellular toxicity, strongly suggesting that the repressing mode of
460 MDs established here for ClpC is also operational in ClpE and ClpL and thus is a
461 more general mechanism for controlling bacterial AAA+ chaperone systems.

462 Severe toxicity of ClpC and ClpE MD mutants qualifies these AAA+ chaperones as
463 targets for antimicrobials. In fact, the deregulation of bacterial proteases
464 represents a novel antibacterial strategy [53,54]. Notably, the *M. tuberculosis* ClpC N-
465 terminal domain was recently identified as target of cyclic peptides with
466 antibacterial activities [55-57]. Although the mode of these drugs and their effects
467 on ClpC function are not understood it is likely that they interfere with ClpC
468 activity control. Our findings presented here open a new route for toxic ClpC
469 deregulation by identifying MDs as crucial regulatory elements and thus drug
470 targets and offering a promising approach to attack multi-drug resistant bacteria.

Materials and Methods

Strains, plasmids and proteins

E. coli strains used were derivatives of MC4100, XL1-blue or DH5α. ClpC, MecA, ClpP were amplified by PCR, inserted into pDS56 and verified by sequencing. Mutant derivatives of ClpC were generated by PCR mutagenesis and standard cloning techniques in pDS56 and were verified by sequencing. Transformation into *B. subtilis* 168 was performed by standard methods [58]. AmyE insertion in *B. subtilis* was checked by plating on agar containing 0.4 % starch (w/v) additionally to appropriate antibiotics, screening for successful loss of α-amylase by staining starch with Lugol's iodine.

ClpC and variants, MecA and ClpP were purified after overproduction from *E. coli* Δ*clpB::kan* cells. GFP-SsrA was purified after overproduction from *E. coli ΔclpX ΔclpP* cells. All proteins were purified using Ni-IDA (Macherey-Nagel) and size exclusion chromatography (Superdex S200, GE Healthcare) following standard protocols. Pyruvate kinase of rabbit muscle, casein and FITC-casein were purchased from Sigma. Protein concentrations were determined with the Bio-Rad Bradford assay.

Biochemical assays

Size exclusion chromatography and multi-angle light scattering.

Complex formation of ClpC (10 μM) was monitored by size exclusion chromatography (SEC, Superose 6 10/300 GL, GE Healthcare). MecA (20 μM),

493 ClpP (20 μM), casein (16.66 μM) and FITC-casein (2.5 μM) were added as
494 indicated. Experiments were run at 25°C in buffer A (50 mM Tris pH 7.5, 25 mM
495 KCl, 20 mM $MgCl_2$) supplemented with 2 mM ATP. Samples were prepared
496 freshly and incubated for 5 minutes with 2 mM ATP prior to injection. Fractions
497 were collected in 96-well plates, aliquots taken and subjected to SDS-PAGE. Gels
498 were stained using SYPRO® Ruby Protein Gel Stain (ThermoFisher) following
499 manufacturer instructions. Band intensities were quantified using ImageJ. To
500 monitor the binding of ClpC to FITC-Casein, the collected fractions were analyzed
501 for FITC fluorescence using FLUOstar Omega (BMG Labtech) with standard FITC
502 filter sets. Chromatography was performed in three independent experiments
503 each and representative results are provided.

504 Complex formation analyzed by SEC was additionally followed by online multi-
505 angle light scattering (MALS) using an Agilent 1260 Infinity II HPLC system
506 connected in series with a 3-angle multi-angle light scattering detector
507 (miniDAWN TREOS II, Wyatt Technology, collection rate of 2 data points per
508 second) and an additional online differential refractive index detector (Optilab T-
509 rEX, Wyatt Technology) for concentration determination. Data analysis was
510 performed using ASTRA 7.1 (Wyatt Technology). Samples were additionally
511 filtered through a 0.2 μm low-protein binding syringe filter (Millex-GV, Merck
512 Millipore Ltd.) before application to the SEC-column.

513 *ATPase activity*

514 The ATPase rate of ClpC and mutants was determined using a coupled-
515 colorimetric assay as described before [9]. The assay was carried out at 2 mM ATP

516 in buffer A including 2 mM DTT at 30°C using a FLUOstar Omega plate reader.
517 The final protein concentrations were as follows: ClpC (1 µM), MecA (1.5 µM),
518 casein (10 µM). In presence of casein MecA concentrations were reduced to 0.2
519 µM .The raw data was analyzed using the following equation:
520

$$\text{ATPase rate} = \frac{1}{\varepsilon(\text{NADH}) \cdot c(\text{ATPase}) \cdot d} \cdot \frac{d(A_{340\,nm})}{dt}$$

521

522 **ε (NADH):** Extinction coefficient at 340 nm for NADH (M^{-1} cm^{-1})
523 **c(ATPase):** Concentration of ATPase (M)
524 **d:** path length (cm)
525 **$d(A_{340\,nm})/dt$:** derivative of the linear graph (slope)
526
527 ATPase rates were calculated from the linear decrease of A_{340} in at least three
528 independent experiments and standard deviations were calculated.
529
530 *Degradation assays*

531 FITC-casein degradation was analyzed using a CLARIOstar plate reader, in black
532 384 well plates (Corning, NBS coated, flat bottom), in buffer A with 2 mM DTT.
533 The final protein concentrations were as follows 0.3 µM FITC-casein, 1 µM ClpC,
534 1.5 µM MecA, 2 µM ClpP. The assay was carried out in the presence of an ATP
535 regenerating system (0.02 mg/mL PK, 3 mM PEP pH 7.5) and 2 mM ATP. For
536 measuring the decrease of FITC-casein fluorescence the filters 483-14 nm (ex)
537 and 530-30 nm (em) were used. For data processing the background in the
538 absence of ClpC was subtracted and the initial fluorescence intensities were set

539 to 1. FITC-casein degradation rates were determined by the initial slopes of the
540 fluorescence signal increase in at least three independent experiments and
541 standard deviations were calculated. Alternatively degradation of FITC-casein (5
542 µM) was monitored by SDS-PAGE followed by Coomassie staining.

543 Degradation of GFP-SsrA (0.2 µM) was performed in buffer A with 2 mM DTT
544 using the following protein concentrations: 1 µM ClpC, 1.5 µM MecA, 2 µM ClpP.
545 Reactions were started by addition of an ATP regenerating system (0.02 mg/mL
546 PK, 3 mM PEP pH 7.5) and 2 mM ATP. GFP fluorescence was monitored with a
547 LS55 spectrofluorimeter (Perkin Elmer) using 400 and 510 nm as excitation and
548 emission wavelengths. Initial GFP-SsrA fluorescence intensity was set as 100 and
549 degradation rates were determined by the initial slopes of fluorescence signal
550 decrease in at least three independent experiments and standard deviations
551 were calculated.

552

553 *Crosslinking*

554 Glutaraldehyde crosslinking was performed by incubating 1 µM ClpC or ClpB
555 buffer B (50 mM HEPES, 25 mM KCL, 10 mM $MgCl_2$, 2 mM DTT, pH 7.5) in
556 absence or presence of 2 mM ATP/ATPγS and 3 µM MecA at 25°C for 15 minutes.
557 Crosslinking was started by adding Glutaraldehyde (Sigma) to a final
558 concentration of 0.1%. Aliquots were taken at indicated time points and
559 crosslinking was quenched by adding Tris (pH 7.5) to a final concentration of 50
560 mM. Samples were subjected to SDS-PAGE and gels stained with SYPRO® Ruby
561 Protein Gel Stain (ThermoFisher).

562 Disulfide crosslinking was performed by incubating 3 µM ClpC in buffer A (in the
563 absence or presence of 2 mM nucleotide). MecA (4.5 µM) was added as indicated
564 MecA and 2 mM β-Mercaptoethanol at 25°C for 5 minutes. Crosslinking was
565 started by addition of copper-phenanthroline to a final concentration of 100 µM.
566 Aliquots were taken and crosslinking was stopped by adding SDS sample buffer
567 without β-mercaptoethanol but containing 4 mM iodacetamide. Samples were
568 boiled and analyzed by SDS-PAGE followed by Coomassie staining.

569 Crosslinking was performed in three independent experiments each and
570 representative results are provided.

571

572 *Anisotropy measurements*

573 FITC-casein (100 nM) was incubated with varying concentrations ClpC in buffer
574 A with 2 mM DTT for 1 h in absence or presence of 2 mM ATPγS. Changes in
575 fluorescence polarization were determined using a CLARIOstar plate reader
576 (BMG Labtech) at 482 and 530 nm excitation and emission wavelengths (Target
577 mP 35).

578 *Western blotting*

579 SDS-PAGEs were transferred to nitrocellulose or PVDF membranes by semi-dry
580 blotting or wet blot transfer. Membranes were subsequently blocked with either
581 3% BSA (w/v) or 5% (w/v) skim milk powder in TBS-T. Custom-made
582 antibodies were used at the following dilutions: anti-ClpC (*B. subtilis*) 1:100.000,
583 anti-ClpE 1:30.000, anti-ClpC (S. aureus) 1:50.000 and anti-MecA 1:30.000. anti-
584 rabbit alkaline phosphatase conjugate (Vector Laboratories) was used as

585 secondary antibody (1:10.000). Blots were developed using NBT/BCIP or ECF™
586 Substrate (GE Healthcare) as reagent and imaged via Image-Reader LAS-4000
587 (Fujifilm). Western blotting was performed in three independent experiments
588 each and representative results are provided.

589

590 **ClpC structure determination by cryo-electron microscopy**

591 *Cryo-electron microscopy*

592 *S. aureus* ClpC WT (6 µM) was incubated for 15 min at room temperature in 25
593 mM Tris-HCl (pH 7.5), 25 mM KCl, 10 mM $MgCl_2$, 1 mM DTT and 2 mM ATPγS.
594 For ClpC-MecA complex formation, *S. aureus* MecA was incubated with ClpC in a
595 3:1 molar ratio. Samples were vitrified with liquid ethane on Quantifoil R2/2
596 grids using a Vitrobot Mark IV (FEI) at 100% humidity, 24°C temperature and
597 blotting time of 3 seconds.
598 Images of ClpC were collected using the EPU software on a Titan Krios TEM (FEI)
599 operating at 300kV, using a Falcon 2 direct electron detector (FEI). Images of
600 ClpC in complex with MecA were collected using the EPU software on a Titan
601 Krios TEM (FEI) operating at 300kV equipped with a Gatan K2 Summit direct
602 electron detector and bioquantum energy filter with 20 eV slit. The defocus
603 range was set between -1 and -3 µm with a total dose of 30 electrons/$Å^2$ in 17
604 frames for ClpC and 50 electrons/$Å^2$ in 40 frames for ClpC-MecA. Pixel size was
605 1.34 Å/pixel for ClpC and 1.37 Å/pixel for ClpC-MecA.
606 *Image processing*
607 Movie frames alignment with dose weighting [59] and CTF estimation [60] was
608 performed on-the-fly using a Scipion suite [61]. ClpC particles were picked with

609 Gautomatch and a dataset of ~90.000 particles from 1100 micrographs was
610 generated. ClpC-MecA complex particles were picked using Gaussian picking in
611 RELION [62] and ~500.000 particles from 2100 micrographs were obtained. The
612 initial datasets were subjected to reference-free 2D classification in order to
613 clean the datasets.
614 Initially, for 3D processing of ClpC (**Supplementary Fig. 4**), the crystal structure
615 of ClpC-MecA [30] low-pass filtered at 60 Å was used, but the dataset failed to
616 refine. Attempts to use *ab initio* models generated with Eman2 [63] also did not
617 result in high-resolution 3D refinement. As the ClpC assembly appeared much
618 larger in size than the ClpC-MecA hexamer, we generated a cylindrical starting
619 model by filtering to 70 Å two copies of ClpC-MecA stuck back to back with the
620 AAA2 rings in contact. With this starting model ClpC refined to 8.4 Å resolution
621 as estimated with the 0.143 FSC criterion, with visible separated helices. The
622 same result was confirmed by generating an *ab-initio* starting model using the
623 SGD method implemented in cryoSPARC [64] and refining the structure within the
624 same program suite. Reconstructions with and without C2 symmetry applied
625 were performed (**Supplementary Fig. 4, g-h)** to a similar resolution and the C2
626 map was used for display as it allows a better visualization of N-domains.

627 For 3D processing of ClpC-MecA (**Supplementary Fig. 5**) the crystal structure of
628 the *B. subtilis* ClpC-MecA complex filtered at 60Å was used (pdb code: 3PXI). A
629 large dataset was initially used, but particles were preferentially oriented so a
630 reduced dataset (~30.000 particles) with balanced angular distribution was
631 used to reduce anisotropy. Both asymmetric and six fold symmetric maps were
632 built. Even though the nominal resolution of the symmetrized map was better,
633 the reconstruction appeared over filtered, thus indicating that artifacts were

634 caused by forced symmetrisation. The final map was reconstructed at 11 Å
635 resolution. Local resolution was evaluated using the local resolution tool of
636 RELION.

637 *Model building and fitting*

638 Models of *S. aureus* ClpC and MecA were generated using Phyre [65]. The N-
639 domain to AAA1 link was refined using the Chimera loops modeller tool [66]. Initial
640 manual fitting was performed and then automatically refines using Imodfit [67].

641

642 **Spot tests**

643 *E. coli* cells harboring plasmid-encoded *clpC* alleles were grown in the absence of
644 IPTG overnight at 30°C. Serial dilutions were prepared, spotted on LB-plates
645 containing different IPTG concentrations and incubated for 24 h at indicated
646 temperatures. *B. subtilis* strains were inoculated with a fresh overnight culture to
647 an OD_{600} of 0.05 and grown to mid-exponential growth phase. Optical densities
648 of all strains were adjusted to OD_{600} of 1, serial dilutions were performed and
649 10 µl (10^{-2} - 10^{-6}) were dropped on agar plates (without or with 100 µM IPTG)
650 and incubated overnight at indicated temperatures. Spot tests were performed in
651 three independent experiments each and representative results are provided.

652

653 **Acknowledgments**

654 K. B. F. was supported by the Hartmut Hoffmann-Berling International Graduate
655 School of Molecular and Cellular Biology (HBIGS). This work was funded by
656 grants of the Deutsche Forschungsgemeinschaft (BB617/17-2 and MO 970/4-2)

657 to B.B. and A.M. and a fellowship of the Hannover School for Biomolecular Drug
658 Research to I.H. and the DFG grants Tu106/8-1 and Tu106/6-2 to K.T. The Cryo-EM
659 facility at the Science for Life Laboratory Stockholm University (M.C.) is
660 supported by grants from the Knut and Alice Wallenberg Foundation and the
661 Family Erling Persson Foundation. We thank Stefan Fleischmann for IT support,
662 Christos Savva for microscopy support, Björn Forsberg and Shintaro Aibara for
663 image-processing discussions, Helen Saibil for support in the early stage of the
664 project and Armgard Janczikowski for technical assistance.

665

666 **Competing interests**: No competing interests declared

667

668 **Author contributions**

669 Conceived and designed experiments: M.C., K.B.F., M.M., J.J., I.H., F.G., D.L., S.G.,
670 K.T., B.B., A.M. Performed experiments: M.C., K.B.F., M.M., J.J., I.H., F.G., D.L., S.G.
671 Analyzed the data: M.C., K.B.F., M.M., J.J., I.H., F.G., D.L., S.G., K.T., B.B., A.M. Wrote
672 the manuscript: M.C., B.B., A.M.

673

674 **References**

675 1. Hanson, P.I. & Whiteheart, S.W. AAA+ proteins: have engine, will work.
676 *Nat Rev Mol Cell Biol* **6**, 519-29 (2005).
677 2. Olivares, A.O., Baker, T.A. & Sauer, R.T. Mechanistic insights into bacterial
678 AAA+ proteases and protein-remodelling machines. *Nat Rev Microbiol* **14**,
679 33-44 (2016).
680 3. Nyquist, K. & Martin, A. Marching to the beat of the ring: polypeptide
681 translocation by AAA+ proteases. *Trends Biochem Sci* **39**, 53-60 (2014).

4. Gur, E., Ottofueling, R. & Dougan, D.A. Machines of destruction - AAA+ proteases and the adaptors that control them. *Subcell Biochem* **66**, 3-33 (2013).
5. Doyle, S.M., Genest, O. & Wickner, S. Protein rescue from aggregates by powerful molecular chaperone machines. *Nat Rev Mol Cell Biol* **14**, 617-29 (2013).
6. Mogk, A., Kummer, E. & Bukau, B. Cooperation of Hsp70 and Hsp100 chaperone machines in protein disaggregation. *Front Mol Biosci* **2**, 22 (2015).
7. Collins, G.A. & Goldberg, A.L. The Logic of the 26S Proteasome. *Cell* **169**, 792-806 (2017).
8. Baker, T.A. & Sauer, R.T. ClpXP, an ATP-powered unfolding and protein-degradation machine. *Biochim Biophys Acta* **1823**, 15-28 (2012).
9. Oguchi, Y. et al. A tightly regulated molecular toggle controls AAA+ disaggregase. *Nat Struct Mol Biol* **19**, 1338-46 (2012).
10. Schirmer, E.C., Homann, O.R., Kowal, A.S. & Lindquist, S. Dominant gain-of-function mutations in Hsp104p reveal crucial roles for the middle region. *Mol Biol Cell* **15**, 2061-72 (2004).
11. Lipinska, N. et al. Disruption of ionic interactions between the nucleotide binding domain 1 (NBD1) and middle (M) domain in Hsp100 disaggregase unleashes toxic hyperactivity and partial independence from Hsp70. *J Biol Chem* **288**, 2857-69 (2013).
12. Mika, F. & Hengge, R. A two-component phosphotransfer network involving ArcB, ArcA, and RssB coordinates synthesis and proteolysis of sigmaS (RpoS) in E. coli. *Genes Dev* **19**, 2770-81 (2005).
13. Bougdour, A., Wickner, S. & Gottesman, S. Modulating RssB activity: IraP, a novel regulator of sigma(S) stability in Escherichia coli. *Genes Dev* **20**, 884-97 (2006).
14. Battesti, A. et al. Anti-adaptors provide multiple modes for regulation of the RssB adaptor protein. *Genes Dev* **27**, 2722-35 (2013).
15. Turgay, K., Hahn, J., Burghoorn, J. & Dubnau, D. Competence in *Bacillus subtilis* is controlled by regulated proteolysis of a transcription factor. *EMBO J.* **17**, 6730-6738 (1998).
16. Schlothauer, T., Mogk, A., Dougan, D.A., Bukau, B. & Turgay, K. MecA, an adaptor protein necessary for ClpC chaperone activity. *Proc Natl Acad Sci U S A* **100**, 2306-11 (2003).
17. Carroni, M. et al. Head-to-tail interactions of the coiled-coil domains regulate ClpB activity and cooperation with Hsp70 in protein disaggregation. *Elife* **3**, e02481 (2014).
18. Heuck, A. et al. Structural basis for the disaggregase activity and regulation of Hsp104. *Elife* **5**(2016).
19. Rosenzweig, R., Moradi, S., Zarrine-Afsar, A., Glover, J.R. & Kay, L.E. Unraveling the mechanism of protein disaggregation through a ClpB-DnaK interaction. *Science* **339**, 1080-3 (2013).
20. Lee, J. et al. Heat shock protein (Hsp) 70 is an activator of the Hsp104 motor. *Proc Natl Acad Sci U S A* **110**, 8513-8 (2013).
21. Turgay, K., Hamoen, L.W., Venema, G. & Dubnau, D. Biochemical characterization of a molecular switch involving the heat shock protein

ClpC, which controls the activity of ComK, the competence transcription factor of Bacillus subtilis. *Genes Dev* **11**, 119-28 (1997).

22. Frees, D., Gerth, U. & Ingmer, H. Clp chaperones and proteases are central in stress survival, virulence and antibiotic resistance of Staphylococcus aureus. *Int J Med Microbiol* **304**, 142-9 (2014).
23. Trentini, D.B. et al. Arginine phosphorylation marks proteins for degradation by a Clp protease. *Nature* **539**, 48-53 (2016).
24. Capestany, C.A., Tribble, G.D., Maeda, K., Demuth, D.R. & Lamont, R.J. Role of the Clp system in stress tolerance, biofilm formation, and intracellular invasion in Porphyromonas gingivalis. *J Bacteriol* **190**, 1436-46 (2008).
25. Msadek, T., Kunst, F. & Rapoport, G. MecB of Bacillus subtilis, a member of the ClpC ATPase family, is a pleiotropic regulator controlling competence gene expression and growth at high temperature. *Proc Natl Acad Sci U S A* **91**, 5788-92 (1994).
26. Kruger, E., Volker, U. & Hecker, M. Stress induction of clpC in Bacillus subtilis and its involvement in stress tolerance. *J Bacteriol* **176**, 3360-7 (1994).
27. Kruger, E., Witt, E., Ohlmeier, S., Hanschke, R. & Hecker, M. The clp proteases of Bacillus subtilis are directly involved in degradation of misfolded proteins. *J Bacteriol* **182**, 3259-65 (2000).
28. Lourdault, K., Cerqueira, G.M., Wunder, E.A., Jr. & Picardeau, M. Inactivation of clpB in the pathogen Leptospira interrogans reduces virulence and resistance to stress conditions. *Infect Immun* **79**, 3711-7 (2011).
29. Mei, Z. et al. Molecular determinants of MecA as a degradation tag for the ClpCP protease. *J Biol Chem* **284**, 34366-75 (2009).
30. Wang, F. et al. Structure and mechanism of the hexameric MecA-ClpC molecular machine. *Nature* **471**, 331-335 (2011).
31. Brotz-Oesterhelt, H. & Sass, P. Bacterial caseinolytic proteases as novel targets for antibacterial treatment. *Int J Med Microbiol* **304**, 23-30 (2014).
32. Conlon, B.P. et al. Activated ClpP kills persisters and eradicates a chronic biofilm infection. *Nature* **503**, 365-70 (2013).
33. Brotz-Oesterhelt, H. et al. Dysregulation of bacterial proteolytic machinery by a new class of antibiotics. *Nat Med* **11**, 1082-7 (2005).
34. Kirstein, J. et al. The antibiotic ADEP reprogrammes ClpP, switching it from a regulated to an uncontrolled protease. *EMBO Molecular Medicine* **1**, 37-49 (2009).
35. Hinnerwisch, J., Fenton, W.A., Furtak, K.J., Farr, G.W. & Horwich, A.L. Loops in the Central Channel of ClpA Chaperone Mediate Protein Binding, Unfolding, and Translocation. *Cell* **121**, 1029-41 (2005).
36. Piszczek, G., Rozycki, J., Singh, S.K., Ginsburg, A. & Maurizi, M.R. The molecular chaperone, ClpA, has a single high affinity peptide binding site per hexamer. *J Biol Chem* **280**, 12221-30 (2005).
37. Siddiqui, S.M., Sauer, R.T. & Baker, T.A. Role of the processing pore of the ClpX AAA+ ATPase in the recognition and engagement of specific protein substrates. *Genes Dev* **18**, 369-74 (2004).
38. Beinker, P., Schlee, S., Groemping, Y., Seidel, R. & Reinstein, J. The N Terminus of ClpB from Thermus thermophilus Is Not Essential for the Chaperone Activity. *J Biol Chem* **277**, 47160-6. (2002).

779 39. Rosenzweig, R. et al. ClpB N-terminal domain plays a regulatory role in
780 protein disaggregation. *Proc Natl Acad Sci U S A* **112**, E6872-81 (2015).
781 40. Kirstein, J. et al. Adaptor protein controlled oligomerization activates the
782 AAA+ protein ClpC. *Embo J* **25**, 1481-91 (2006).
783 41. Persuh, M., Turgay, K., Mandic-Mulec, I. & Dubnau, D. The N and the C-
784 terminal domains of MecA recognize different partners in the competence
785 molecular switch. *Mol. Microbiol.* **33**, 886-894 (1999).
786 42. Flynn, J.M. et al. Overlapping recognition determinants within the ssrA
787 degradation tag allow modulation of proteolysis. *Proc Natl Acad Sci U S A*
788 **98**, 10584-9 (2001).
789 43. Liu, J. et al. Structural dynamics of the MecA-ClpC complex: a type II AAA+
790 protein unfolding machine. *J Biol Chem* **288**, 17597-608 (2013).
791 44. Lee, S. et al. The Structure of ClpB. A Molecular Chaperone that Rescues
792 Proteins from an Aggregated State. *Cell* **115**, 229-40 (2003).
793 45. Guo, F., Maurizi, M.R., Esser, L. & Xia, D. Crystal structure of ClpA, an
794 Hsp100 chaperone and regulator of ClpAP protease. *J Biol Chem* **277**,
795 46743-52. (2002).
796 46. Monroe, N., Han, H., Shen, P.S., Sundquist, W.I. & Hill, C.P. Structural basis
797 of protein translocation by the Vps4-Vta1 AAA ATPase. *Elife* **6**(2017).
798 47. Gerth, U. et al. Fine-tuning in regulation of Clp protein content in Bacillus
799 subtilis. *J Bacteriol* **186**, 179-91 (2004).
800 48. Miethke, M., Hecker, M. & Gerth, U. Involvement of Bacillus subtilis ClpE in
801 CtsR degradation and protein quality control. *J Bacteriol* **188**, 4610-9
802 (2006).
803 49. Seyffer, F. et al. Hsp70 proteins bind Hsp100 regulatory M domains to
804 activate AAA+ disaggregase at aggregate surfaces. *Nat Struct Mol Biol* **19**,
805 1347-55 (2012).
806 50. Kirstein, J., Dougan, D.A., Gerth, U., Hecker, M. & Turgay, K. The tyrosine
807 kinase McsB is a regulated adaptor protein for ClpCP. *EMBO J* **26**, 2061-70
808 (2007).
809 51. Preissler, S. et al. Physiological modulation of BiP activity by trans-
810 protomer engagement of the interdomain linker. *Elife* **4**, e08961 (2015).
811 52. Mueller-Cajar, O. et al. Structure and function of the AAA+ protein CbbX, a
812 red-type Rubisco activase. *Nature* **479**, 194-9 (2011).
813 53. Malik, I.T. & Brotz-Oesterhelt, H. Conformational control of the bacterial
814 Clp protease by natural product antibiotics. *Nat Prod Rep* (2017).
815 54. Culp, E. & Wright, G.D. Bacterial proteases, untapped antimicrobial drug
816 targets. *J Antibiot (Tokyo)* **70**, 366-377 (2017).
817 55. Schmitt, E.K. et al. The natural product cyclomarin kills Mycobacterium
818 tuberculosis by targeting the ClpC1 subunit of the caseinolytic protease.
819 *Angew Chem Int Ed Engl* **50**, 5889-91 (2011).
820 56. Gao, W. et al. The Cyclic Peptide Ecumicin Targeting ClpC1 Is Active
821 against Mycobacterium tuberculosis In Vivo. *Antimicrob Agents*
822 *Chemother* **59**, 880-9 (2015).
823 57. Gavrish, E. et al. Lassomycin, a ribosomally synthesized cyclic peptide,
824 kills mycobacterium tuberculosis by targeting the ATP-dependent
825 protease ClpC1P1P2. *Chem Biol* **21**, 509-18 (2014).
826 58. Anagnostopoulos, C. & Spizizen, J. Requirements for Transformation in
827 Bacillus Subtilis. *J Bacteriol* **81**, 741-6 (1961).

59. Zheng, S.Q. et al. MotionCor2: anisotropic correction of beam-induced motion for improved cryo-electron microscopy. *Nat Methods* **14**, 331-332 (2017).
60. Rohou, A. & Grigorieff, N. CTFFIND4: Fast and accurate defocus estimation from electron micrographs. *J Struct Biol* **192**, 216-21 (2015).
61. de la Rosa-Trevin, J.M. et al. Scipion: A software framework toward integration, reproducibility and validation in 3D electron microscopy. *J Struct Biol* **195**, 93-9 (2016).
62. Scheres, S.H. RELION: implementation of a Bayesian approach to cryo-EM structure determination. *J Struct Biol* **180**, 519-30 (2012).
63. Tang, G. et al. EMAN2: an extensible image processing suite for electron microscopy. *J Struct Biol* **157**, 38-46 (2007).
64. Punjani, A., Rubinstein, J.L., Fleet, D.J. & Brubaker, M.A. cryoSPARC: algorithms for rapid unsupervised cryo-EM structure determination. *Nat Methods* **14**, 290-296 (2017).
65. Kelley, L.A. & Sternberg, M.J. Protein structure prediction on the Web: a case study using the Phyre server. *Nat Protoc* **4**, 363-71 (2009).
66. Pettersen, E.F. et al. UCSF Chimera--a visualization system for exploratory research and analysis. *J Comput Chem* **25**, 1605-12 (2004).
67. Lopez-Blanco, J.R. & Chacon, P. iMODFIT: efficient and robust flexible fitting based on vibrational analysis in internal coordinates. *J Struct Biol* **184**, 261-70 (2013).

860 **Figure legends**

861 **Figure 1**

862 ClpC MD mutants exhibit adaptor-independent proteolytic activity. (**A/B**) FITC-
863 casein degradation was monitored in the presence of ClpP (P) only, or in
864 presence of ClpC wild type (WT, ± MecA) and indicated MD mutants (without
865 MecA). Degradation rates were determined from the initial linear increase of
866 FITC fluorescence. (**C-E**) GFP-SsrA degradation was monitored in the presence of
867 ClpP and indicated ClpC variants. Deletion of the N-terminal domain (ΔN)
868 unleashes high proteolyic activity of MD mutants. GFP-SsrA degradation rates
869 were determined from the initial linear decrease of GFP-SsrA fluorescence.

870

871 **Figure 2**

872 ClpC MD mutants exhibit increased basal ATPase activity that can be stimulated
873 by substrate. (**A**) ATPase activities of ClpC wild type (WT) and indicated deletion
874 variants (ΔN, ΔM) and MD mutants were determined in absence and presence of
875 MecA. (**B**) ATPase activities of ClpC wild type (WT, ± MecA) and indicated MD
876 mutants were determined in absence and presence of substrate casein. ATPase
877 activities determined without casein were set as 1 and the relative increase of
878 ATP hydrolysis in presence of casein was determined (stimulation factor).

879

880

881

882 **Figure 3**

883 Cryo-EM structures of *S. aureus* ClpC-ATPγS with and without MecA. (**A**)
884 Overview of ClpC 3D density map showing two open spirals that interact in a
885 head-to-head manner. (**B**) ClpC density map coloured by domains. Head-to-head
886 interactions between MDs (green) of each helical assembly are key contacts
887 stabilizing the ClpC resting state. ClpC domain organization is given, including an
888 N-terminal domain (NT), two AAA-domains (AAA-1, AAA-2) and the inserted
889 coiled-coil M-domain (MD). (**C**) Details of fitting for each ClpC subdomain. (**D**)
890 Zoomed view into MD-MD contacts highlighting conserved MD residues involved
891 in interactions. (**E**) Structure of the ClpC-MecA complex. Fitted atomic model
892 coloured by ClpC domains as in b and MecA C-terminal domains (purple).
893 Density for MecA N-terminal domains is indicated.

894

895 **Figure 4**

896 Disulfide crosslinking demonstrates MecA-sensitive head-to-head MD contacts.
897 (**A**) Disulfide crosslinking of ClpC-C311T/E437C under oxidizing conditions was
898 performed in presence of ATPγS or ATP without or with MecA and analyzed by
899 subsequent non-reducing SDS-PAGE. A model of head-to-head interacting MDs is
900 given and the position of E437 is indicated. (**b**) Disulfide crosslinking of ClpC-
901 C311T/E437C and ClpC-C311T/F436A/E437C was performed in presence of
902 ATPγS under oxidizing (+ $Cu(Phe_3)$) and reducing (+ β-mercaptoethanol) conditions
903 and analyzed by subsequent non-reducing SDS-PAGE.

904

905 **Figure 5**

906 ClpC forms a large, inactive resting state that is sensitive to MecA and MD
907 mutation. (**A**) Glutaraldehyde crosslinking of ClpC-E280A/E618A (ClpC-DWB)
908 and a respective MD mutant variant (F436A) was performed in absence and
909 presence of ATP without and with MecA as indicated. Crosslinking of *E. coli* ClpB
910 in presence of ATPγS served as reference defining crosslinked hexameric
911 assemblies. Crosslink products were analyzed by SDS-PAGE. (**B**) Oligomeric
912 states of ClpC-DWB and ClpC-F436A-DWB were determined in absence and
913 presence of ATP. Addition of MecA and casein is indicated. Elution fractions were
914 analyzed by SDS-PAGE and quantified. Positions of peak fractions of a protein
915 standard and ClpB-E279A/E678A hexamers (+ATP) are indicated. (**C**)
916 Micrograph of ClpC-F436A sample in presence of casein (top). Examples of single
917 particles are circled. 2D class averages of ClpC-F436A (bottom). Scale bar is 10
918 nm. (**D**) Binding of FITC-casein to ClpC-DWB and ClpC-F436A-DWB was analyzed
919 in presence of ATP by size exclusion chromatography. FITC-casein fluorescence
920 of elution fractions was quantified. Positions of peak fractions of a protein
921 standard and ClpB-E279A/E678A hexamers (+ATP) are indicated.

922

923 **Figure 6**

924 Loss of ClpC activity control is toxic *in vivo*. (**A**) *E. coli* cells constitutively
925 expressing *S. aureus clpP* and harboring the indicated plasmid-encoded *clpC*
926 alleles under control of an IPTG-regulatable promoter were grown overnight at
927 30°C and adjusted to OD_{600} of 1. Serial dilutions (10^{-2} – 10^{-6}) were spotted on LB

928 plates containing the indicated IPTG concentrations and incubated at 30°C, 37°C
929 or 40°C for 24 h. (**B**) *B. subtilis ΔclpC* control cells and *ΔclpC* mutant cells
930 harboring a *clpC* wild type (WT) or MD mutant (F436A) copy integrated at the
931 *amyE*-locus under control of an IPTG-regulatable promoter were grown at 30°C
932 to OD600 =1. Serial dilutions (10^{-2} – 10^{-6}) were spotted on LB plates without or
933 with 100 μM IPTG and incubated at 30°C, 37°C or 50°C for 24 h. (**C**) Sequence
934 alignment of MDs from ClpC, ClpE and ClpL proteins. A highly conserved
935 aromatic residue located at the tip of the coiled-coil structure is highlighted. (**D**)
936 *B. subtilis* cells harboring an extra *clpE* wild type (WT) or MD mutant (Y344A)
937 copy integrated at the *amyE*-locus under control of an IPTG-regulatable
938 promoter were grown at 30°C to OD600 =1. Serial dilutions (10^{-2} – 10^{-6}) were
939 spotted on LB plates without or with 100 μM IPTG and incubated at 30°C, 37°C
940 or 50°C for 24 h.

941

942 **Figure 7**

943 Regulatory coiled-coil MDs repress AAA+ protein activities by different
944 mechanisms. ClpB is kept in a low activity resting state by long MDs forming a
945 repressive belt around the hexameric AAA ring. MDs are kept in place by head-
946 to-tail interactions between adjacent coiled-coils. In contrast, the ClpC resting
947 state is formed by head-to-head MD contacts, allowing for assembly of two open
948 ClpC spirals. Adaptor proteins of ClpB (DnaK) and ClpC (MecA) break MD
949 contacts by binding to MD sites crucial for MD interactions. This results in AAA+
950 protein activation by releasing MD repression on ATPase activity (ClpB) or
951 allowing for formation of active hexamers (ClpC).

Figure 1

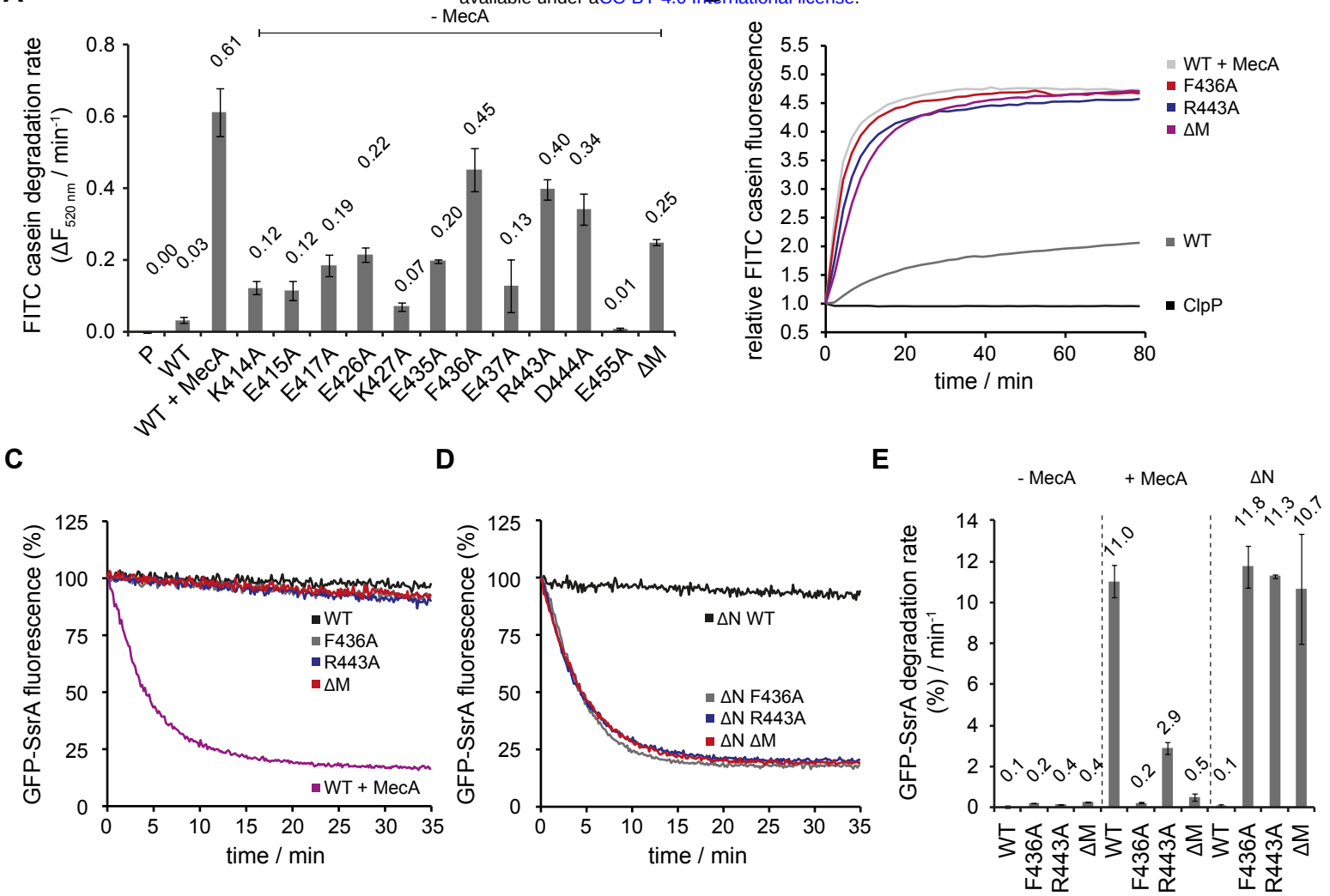

Figure 2

A

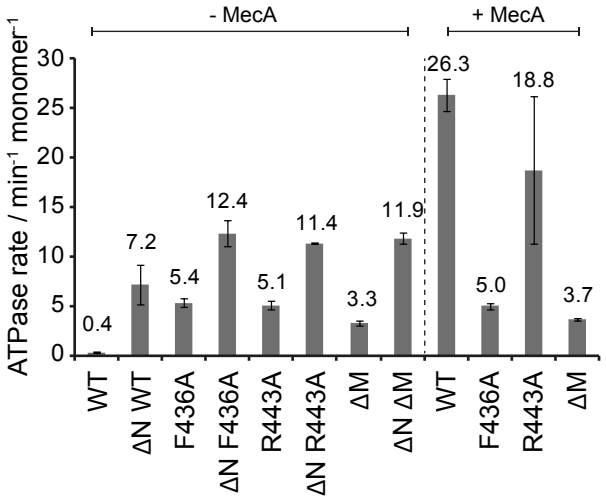

B

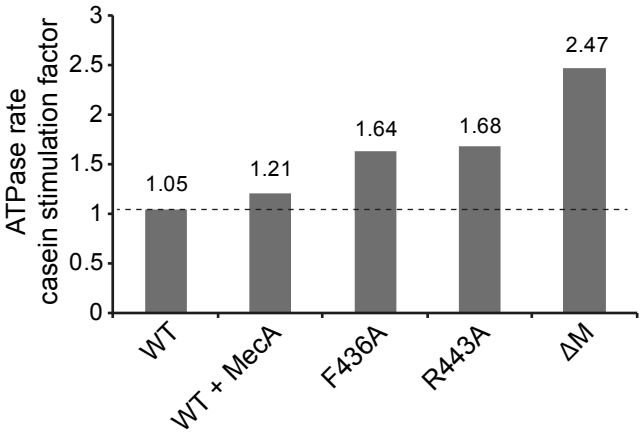

Figure 3

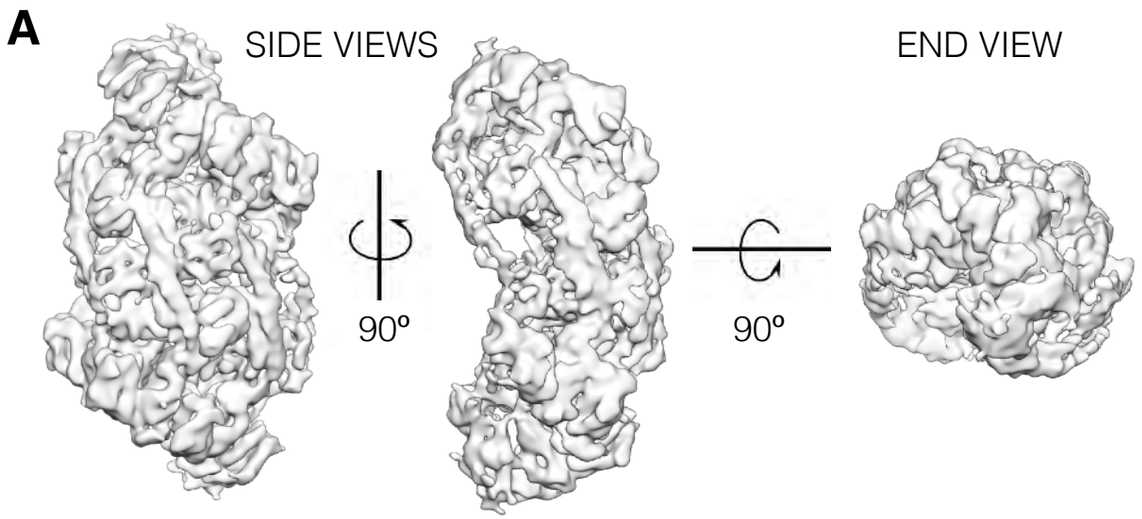
A
SIDE VIEWS
END VIEW
90°
90°

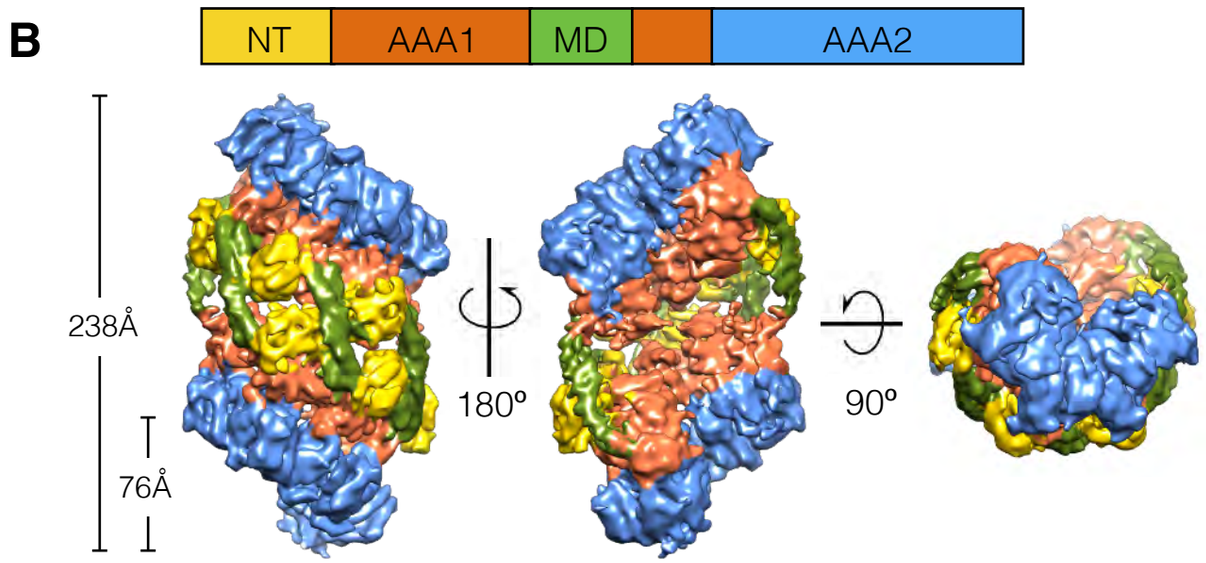
B
NT
AAA1
MD
AAA2
238Å
76Å
180°
90°

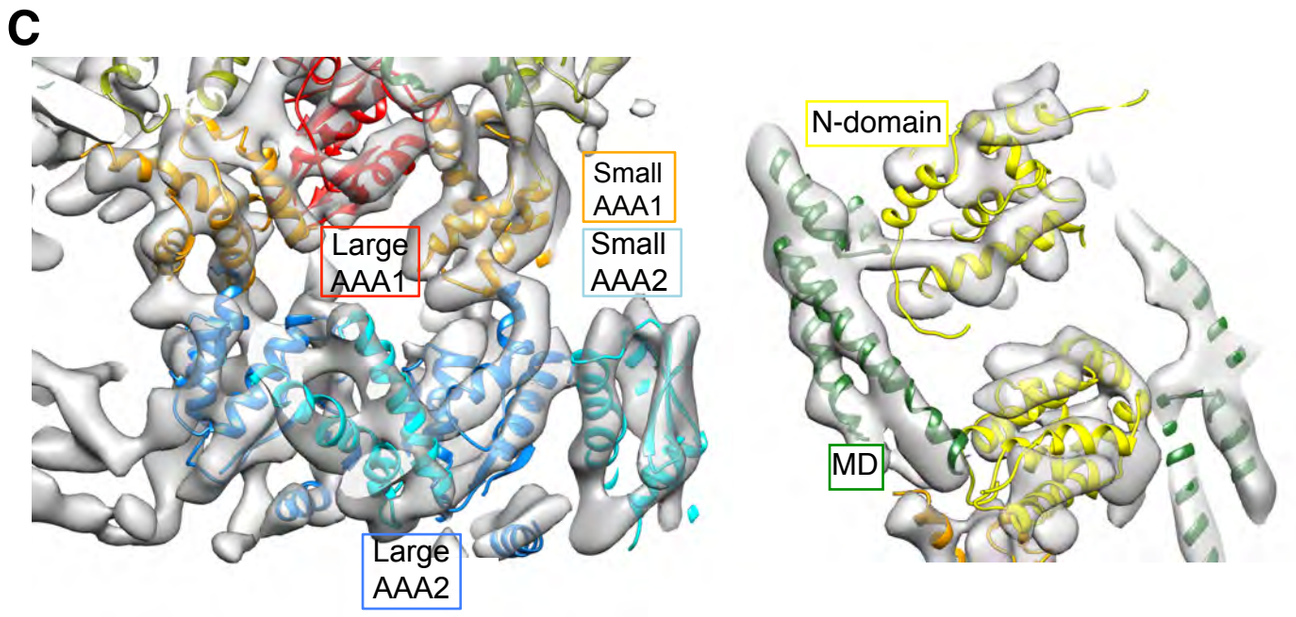
C
Small AAA1
Large AAA1
Small AAA2
Large AAA2
N-domain
MD

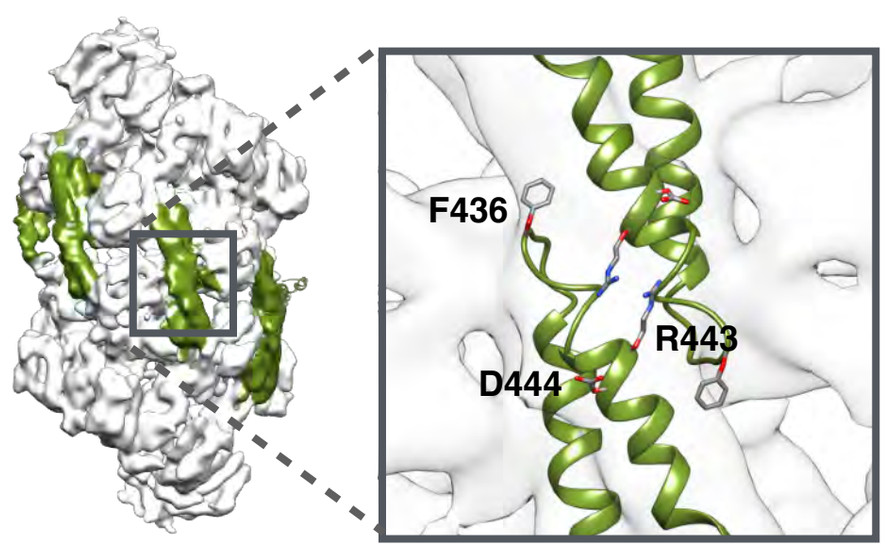
D
F436
R443
D444

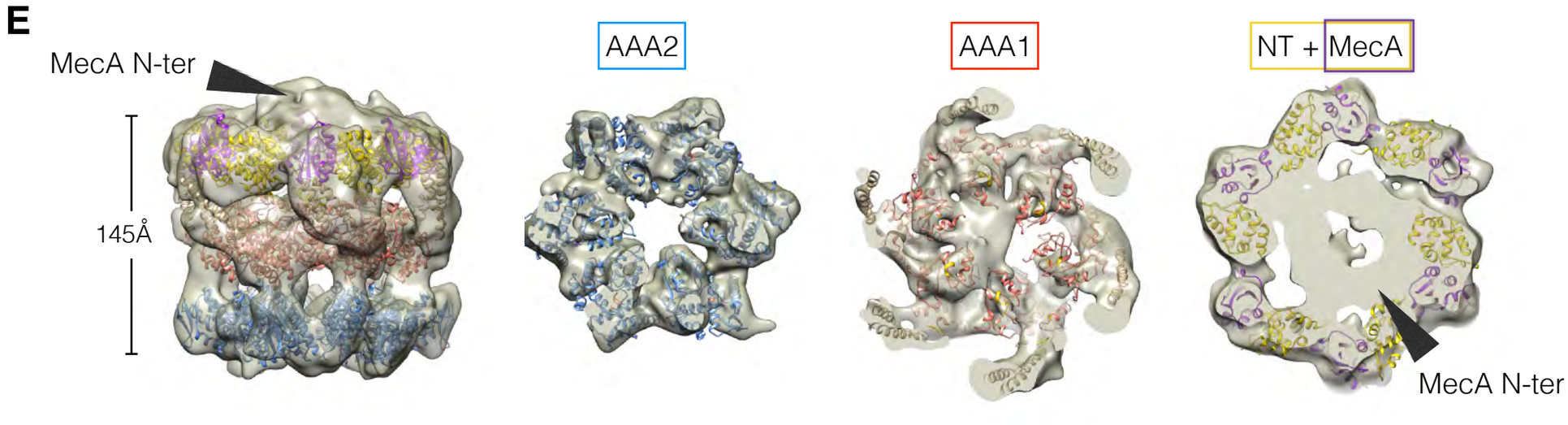
E
MecA N-ter
145Å
AAA2
AAA1
NT + MecA
MecA N-ter

Figure 4

A

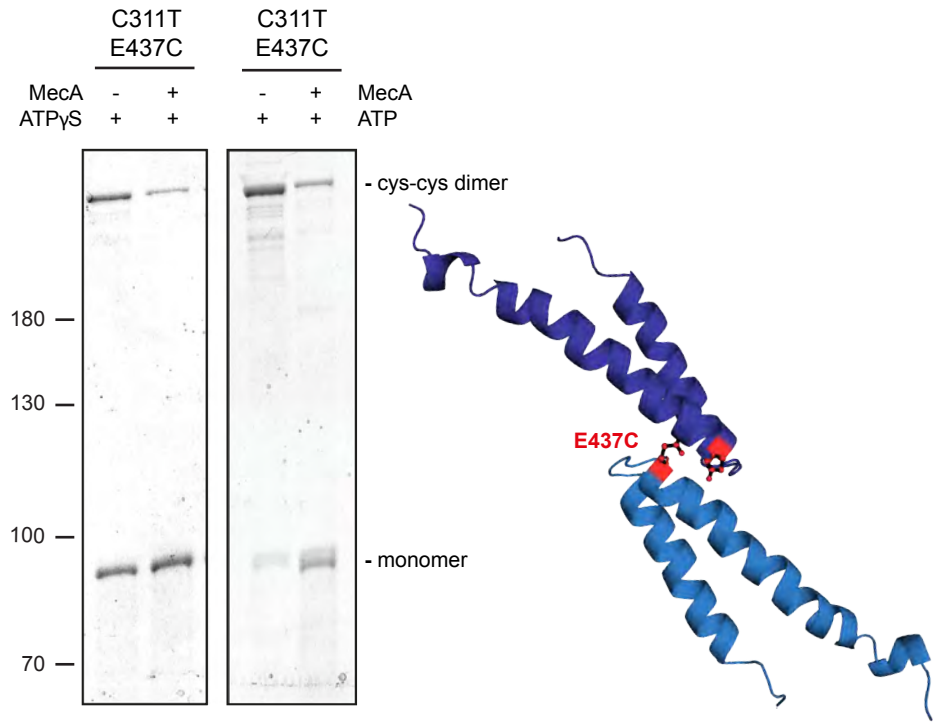

B

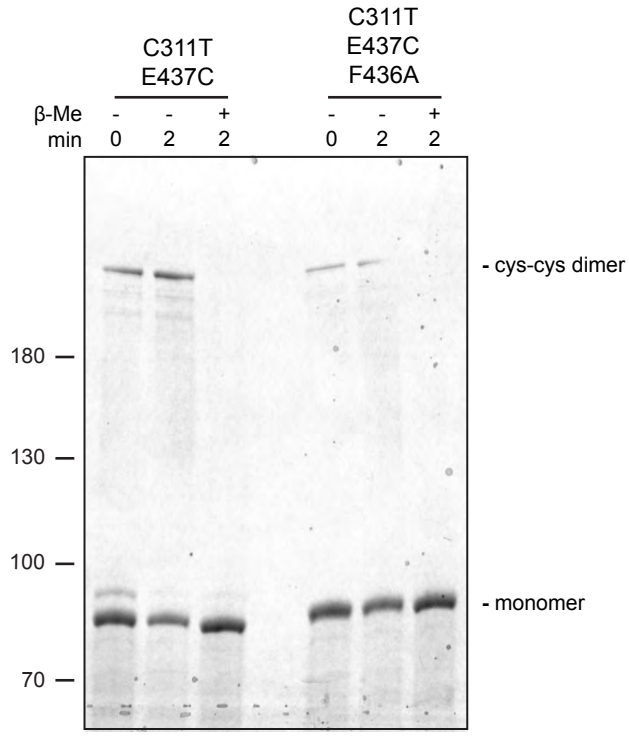

Figure 5

A

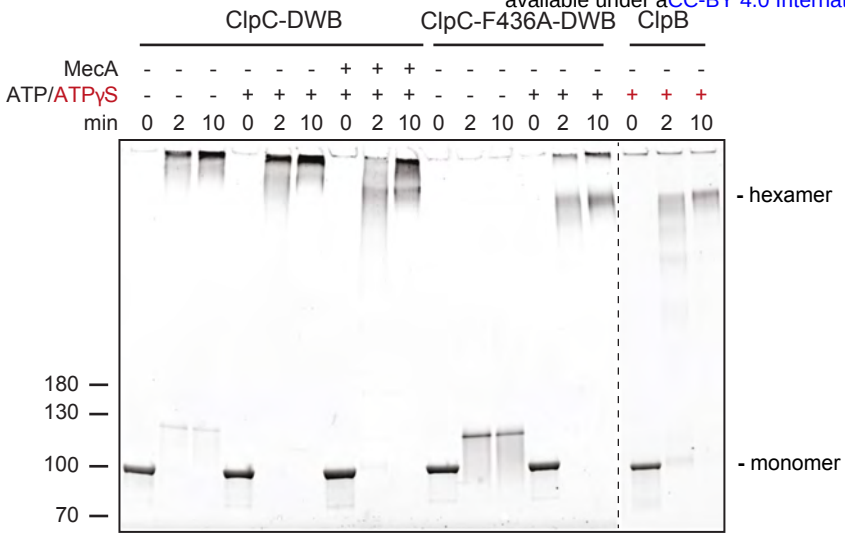

B

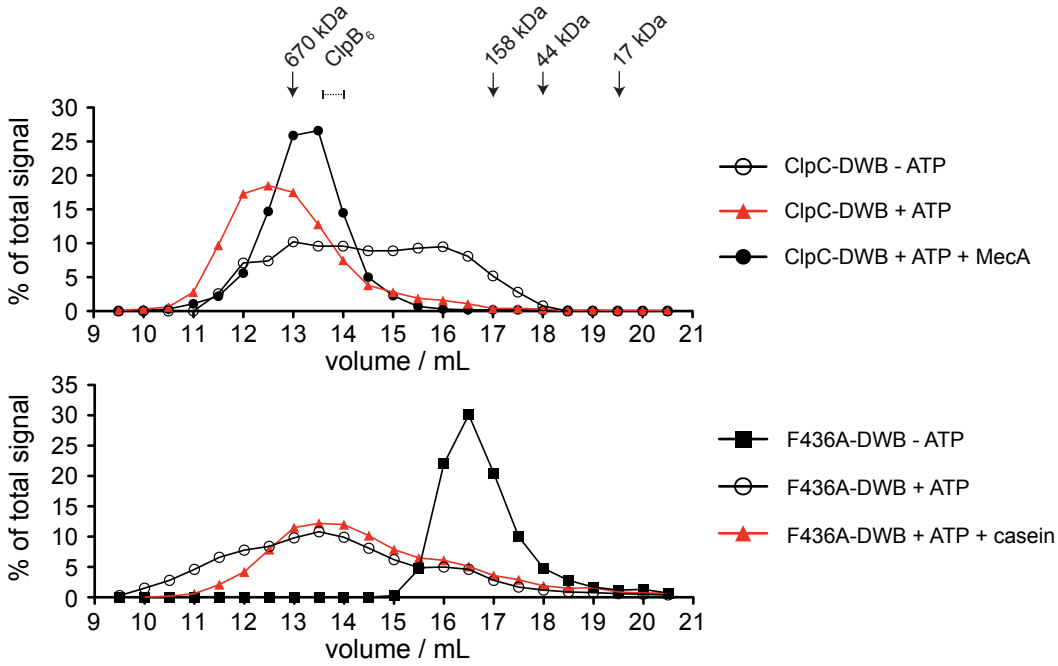

C

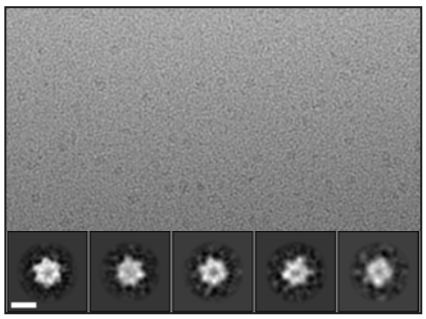

D

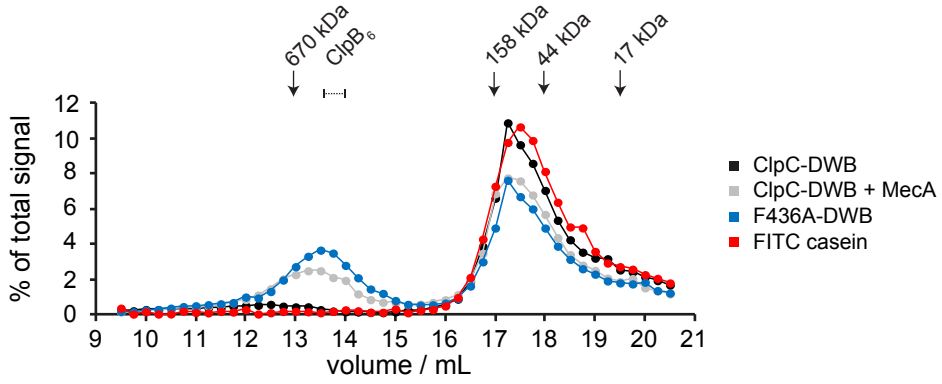

Figure 6

A

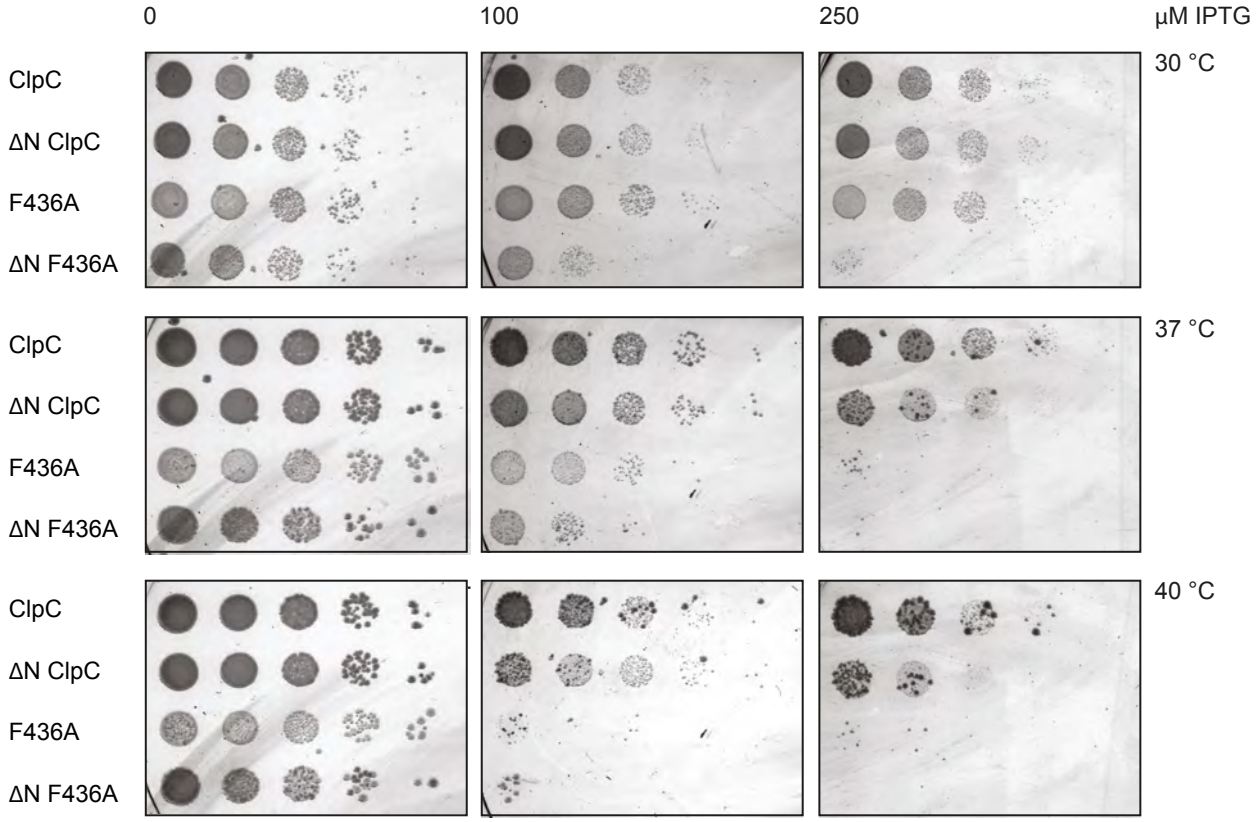

B

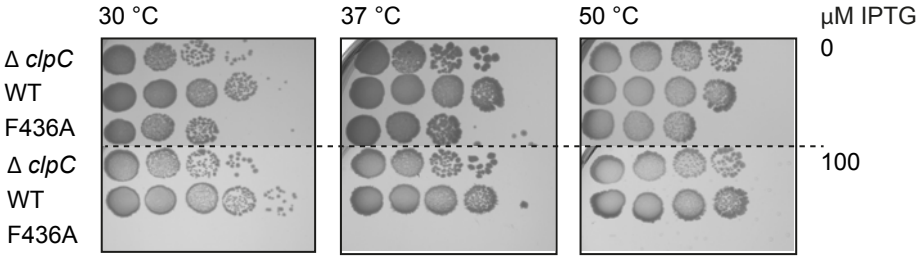

C

```
S. aureus ClpC          410 PNNLKEIEQEIEKVKNEKDAAVHAQEFENAANLRDKQTKLEKQYEEAK 457
M. tuberculosis ClpC    418 PPDLREFDEKIAEARREKESAIDAQDFEKAASLRDREKTLVAQRAERE 465
B. subtilis ClpC        410 PPNLKELEQKLDEVRKEKDAAVQSQEFEKAASLRDTEQRLREQVEDTK 457
B. subtilis ClpE        320 --NDEDAAERLTAIEAEKTKALEEENYELAAKLRDEELALEKKLNS-- 363
S. pneumoniae ClpE      360 --DPKVIDQRLIEAENLKSQATREEDFEKAAYFRDQIAKYKEMQKK-- 403
S. aureus ClpL          331 --DKVETEKRISELENDKRKAVSAEEYKKADDIQNEIKSLQDKLEN-- 374
S. pneuomoniae ClpL     326 --DVHAVEREIETEKDKQEKAVEAEDFEAALNYKTRIAELERKIEN-- 369
                                ..:   .  :  *   :::: *   :
```

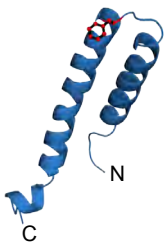

D

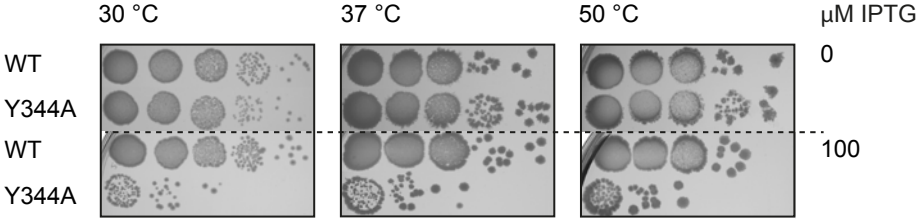

Figure 7